

Beamspace MU-MIMO for High-Density Gigabit Small Cell Access at Millimeter-Wave Frequencies

John Brady and Akbar Sayeed
Electrical and Computer Engineering
jhbrady@wisc.edu, akbar@enr.wisc.edu
University of Wisconsin - Madison

Abstract—Through orders-of-magnitude larger bandwidths and small wavelengths that enable high-dimensional multiple-input multiple-output (MIMO) operation, millimeter-wave (mm-wave) systems operating from 30-300 GHz provide a unique opportunity for meeting the exploding capacity demands on wireless networks. Previously, the performance of multiuser MIMO (MU-MIMO) precoders that exploit the concept of beamspace MIMO (B-MIMO) communication – multiplexing data onto orthogonal spatial beams – was explored for access points (APs) equipped with n -dimensional uniform linear arrays (ULAs). It was shown that APs using reduced complexity B-MIMO transceivers achieve near-optimal performance with complexity that tracks the number of mobile stations (MSs). In this paper we explore the application of the reduced complexity B-MIMO transceivers to APs equipped with uniform planar arrays (UPAs) serving small cells. First, we apply B-MIMO theory to develop a framework for analyzing the small cell in terms of the orthogonal beam footprints. We then examine the effect of several parameters on the system performance and demonstrate that the low-complexity transceivers enable 1000s of Gigabit/s aggregate rates in mm-wave small cells serving hundreds of MSs.

Index Terms—millimeter-wave wireless, Gigabit wireless, high-dimensional MIMO, massive MIMO, beamforming

I. INTRODUCTION

Capacity demands on wireless networks are growing exponentially with the proliferation of data intensive wireless devices. In wireless networks operating below 5 GHz, small cells [1]–[4] are being pursued for addressing this challenge through increased re-use of the spectrum. Emerging millimeter-wave (mm-wave) systems, operating from 30-300 GHz represent a complementary, synergistic opportunity due to the orders-of-magnitude larger available bandwidths as well as high-dimensional multiple-input multiple-output (MIMO) operation due to the small wavelengths that enable packing many more critically (half-wavelength) spaced antennas in a given antenna aperture [5], [6]. The large number of MIMO degrees of freedom can be exploited for a number of critical capabilities, including [5]–[8]: higher antenna/beamforming gain; higher spatial multiplexing gain; and highly directional communication with narrow beams.

The extremely *narrow beamwidths* at mm-wave (Fig. 1(a)) offer a powerful, complementary alternative to small cells through *dense spatial multiplexing*: reuse of spectral resources

across distinct beams [5], [6]. The spatial multiplexing gain, coupled with the larger bandwidths, promises unprecedented gains in network throughput and spectral efficiency even over larger spatial scales due to the large *antenna directivity gains* (Fig. 1(b)). Fig. 1(c) shows idealized spectral efficiency upper bounds for downlink communication from an access point (AP) with a $2.5'' \times 12''$ antenna. While at 3 GHz a maximum of 14 mobile stations (MSs) can be spatially multiplexed, at 80 GHz orders-of-magnitude improvements are possible in signal-to-noise ratio (SNR) due to antenna gain, and in spectral efficiency due to spatial multiplexing gain. Indeed, 100-50,000 Gigabits/s (Gbps) aggregate rates (over 100-300 MSs) seem attainable with the 1-10 GHz of available mm-wave bandwidth.

In [9], it was shown for APs equipped with uniform linear arrays (ULAs) of critically (half-wavelength) spaced antennas that linear transceivers exploiting the concept of beamspace MIMO (B-MIMO) communication – multiplexing data onto orthogonal spatial beams – and beam selection achieve near-optimal performance with complexity that tracks the number of MSs. In this paper we explore the performance of the reduced-complexity B-MIMO transceivers for APs equipped with uniform planar arrays (UPAs) in small cells. Using a realistic line of sight (LoS) channel model, we examine the impact of several system parameters and demonstrate that the low-complexity B-MIMO transceivers are capable of providing 1000s of Gbps aggregate rates over hundreds of MSs in mm-wave small cell networks.

II. SYSTEM MODEL

We focus on an access points equipped with a multi-antenna array communicating with K single-antenna MSs. We examine the more challenging scenario of downlink communication - the uplink problem is well-studied [10] and can be formulated easily along the lines discussed here. Let the AP be equipped with a UPA of dimension $n = n_{az} \times n_{el}$, where n_{az} and n_{el} are the number of antennas in the azimuth and elevation dimensions. We note that this model also captures the performance of APs equipped with continuous aperture antennas that perform analog beamforming [5], [6]. The received signal at the k^{th} MS is given by

$$r_k = \mathbf{h}_k^H \mathbf{x} + w_k$$

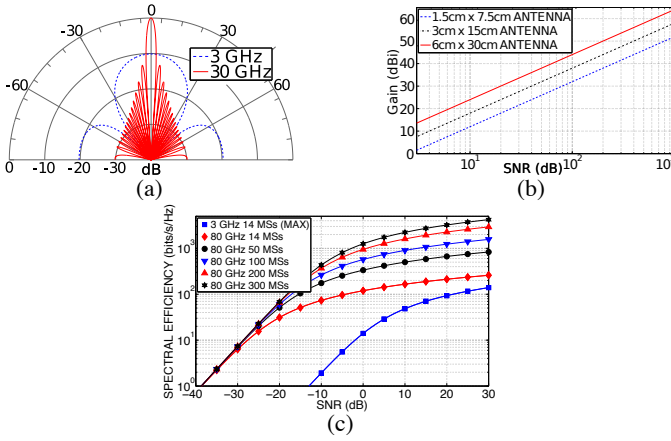


Fig. 1: (a) Antenna beam patterns for a 6" antenna at 3 GHz vs. 30GHz. (b) Antenna gain vs. frequency. (c) Potential multiuser spectral efficiency gains due to spatial multiplexing at 80 GHz vs. 3GHz with a $2.5'' \times 12''$ antenna.

where $\mathbf{x} = [x_1, \dots, x_n]^T$ is the $n \times 1$ transmitted signal, \mathbf{h}_k is the $n \times 1$ channel vector, and $w_k \sim \mathcal{CN}(0, \sigma^2)$ is additive white Gaussian noise (AWGN). Stacking the signals for all MSs in a $K \times 1$ vector $\mathbf{r} = [r_1, \dots, r_K]^T$ we get the antenna domain system equation

$$\mathbf{r} = \mathbf{H}^H \mathbf{x} + \mathbf{w}, \quad \mathbf{H} = [\mathbf{h}_1, \dots, \mathbf{h}_K] \quad (1)$$

where \mathbf{H} is the $n \times K$ channel matrix that characterizes the system and $\mathbf{w} \sim \mathcal{CN}(0, \sigma^2 \mathbf{I})$. We consider systems that use linear precoding for the transmitted signal, $\mathbf{x} = \mathbf{G}\mathbf{s} = \sum_{i=1}^K \mathbf{g}_i s_i$, where \mathbf{s} is the $K \times 1$ vector of independent symbols for different MSs. The overall system equation becomes

$$\mathbf{r} = \mathbf{H}^H \mathbf{G}\mathbf{s} + \mathbf{w}, \quad E[\|\mathbf{x}\|^2] = \text{tr}(\mathbf{G}\mathbf{\Lambda}_s \mathbf{G}^H) \leq \rho \quad (2)$$

where the second equality represents the constraint on total transmit power, ρ , and $\mathbf{\Lambda}_s = E[\mathbf{s}\mathbf{s}^H]$ denotes the diagonal correlation matrix of \mathbf{s} .

A. Channel Model

The channel matrix \mathbf{H} governs the performance of MU-MIMO links. For critically sampled, n -dimensional UPAs the channel can be accurately modeled via the 2D $n \times 1$ array steering vector (SV)

$$\mathbf{a}_n(\theta^{\text{az}}, \theta^{\text{el}}) = \mathbf{a}_{n_{\text{az}}}(\theta^{\text{az}}) \otimes \mathbf{a}_{n_{\text{el}}}(\theta^{\text{el}}) \quad (3)$$

where $\mathbf{a}_n(\theta)$ is the 1D ULA SV given by

$$\mathbf{a}_n(\theta) = [e^{-j2\pi\theta i}]_{i \in \mathcal{I}(n)}, \quad \theta = 0.5 \sin(\phi) \quad (4)$$

where $\mathcal{I}(n) = \{\ell - (n-1)/2 : \ell = 0, 1, \dots, n-1\}$ is a symmetric set of indices centered around 0. The SV $\mathbf{a}_n(\theta)$ represents a discrete, complex spatial sinusoid whose spatial frequency $\theta \in [-0.5, 0.5]$ corresponds to a point source in the direction $\phi \in [-\pi/2, \pi/2]$ [5], [6], [11].

Due to the highly directional, quasi-optical nature of propagation at mm-wave, LoS propagation is predominant, with possibly a sparse set of single-bounce multipath components [12]. We assume that LoS paths exist for all MSs. Let $(\theta_{k,0}^{\text{az}}, \theta_{k,0}^{\text{el}})$, $k = 1, \dots, K$, denote the LoS spatial frequencies for the K MSs. The LoS channel for the k^{th} MS is

$\mathbf{h}_k = \beta_{k,0} \mathbf{a}_n(\theta_{k,0}^{\text{az}}, \theta_{k,0}^{\text{el}})$, where $\beta_{k,0}$ is the complex path loss. In general, for sparse multipath channels

$$\mathbf{h}_k = \beta_{k,0} \mathbf{a}_n(\theta_{k,0}^{\text{az}}, \theta_{k,0}^{\text{el}}) + \sum_{i=1}^{N_p} \beta_{k,i} \mathbf{a}_n(\theta_{k,i}^{\text{az}}, \theta_{k,i}^{\text{el}}) \quad (5)$$

where $\{\theta_{k,i}^{\text{az}}, \theta_{k,i}^{\text{el}}\}$ denote the path spatial frequencies and $\{\beta_{k,i}\}$ represents the complex path loss associated with the different paths for the k^{th} MS. The amplitudes $|\beta_{k,i}|$ for multipath components are typically 5 to 10dB weaker than the LoS component $|\beta_{k,0}|$ [12].

In this paper, we focus on the purely LoS channel induced by propagation between the AP and K MSs located within a specified sector of a small cell (e.g for 120° sectors in azimuth, three APs will cover 360°). The UPA is centered at the origin in the $y-z$ plane and rotated by an angle of $-\psi$ in the $x-z$ plane about the y axis. The MSs are located a distance h below the AP with polar coordinates in the $x-y$ plane $R_{\min} \leq R_k \leq R_{\max}$ and $-\eta_{\max} \leq \eta_k \leq \eta_{\max}$. Fig. 2a shows an illustration of the cell geometry. The LoS spatial frequencies in azimuth and elevation of the k^{th} MS can be related to the MS coordinates (R_k, η_k) through

$$\theta_k^{\text{az}} = \frac{1}{2} \frac{R_k \sin \eta_k}{\sqrt{(R_k \cos \eta_k \cos \psi + h \sin \psi)^2 + R_k^2 \sin^2 \eta_k}} \quad (6)$$

$$\theta_k^{\text{el}} = \frac{1}{2} \frac{R_k \cos \eta_k \sin \psi - h \cos \psi}{\sqrt{R_k^2 \cos^2 \eta_k + h^2}}. \quad (7)$$

The LoS path loss is $\beta_k = |\beta_k| e^{j\phi_k}$, where $|\beta_k|$ is calculated using the Friis transmission formula [13] as

$$|\beta_k|^2 = \frac{D_o(\theta_k^{\text{az}}, \theta_k^{\text{el}}) \lambda^2}{16\pi^2 (h^2 + R_k^2)} \quad (8)$$

where λ is the operating wavelength and $D_o(\theta_k^{\text{az}}, \theta_k^{\text{el}})$ is the array directivity in the direction $(\theta_k^{\text{az}}, \theta_k^{\text{el}})$ [14].

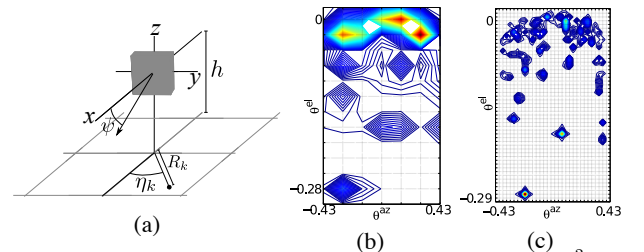


Fig. 2: (a) Plot of the cell geometry (b) Zoomed in contour plot of $\sum_k |\mathbf{h}_{b,k}|^2$ reshaped into a $n_{\text{az}} \times n_{\text{el}}$ matrix for a UPA of dimension $(n_{\text{az}}, n_{\text{el}}) = (7, 39)$, $K = 100$ MSs, and $p = K$ (c) Zoomed in contour plot of $\sum_k |\mathbf{h}_{b,k}|^2$ reshaped into a $n_{\text{az}} \times n_{\text{el}}$ matrix for a UPA of dimension $(n_{\text{az}}, n_{\text{el}}) = (32, 163)$, $K = 100$ MSs, and $p = 16K$. In (b) and (c) the grid lines represents the beamspace sampling points.

B. Beamspace MIMO

The beamspace MIMO system representation is obtained from (1) via fixed beamforming at the transmitter. The columns of the beamforming matrix, \mathbf{U}_o , are SVs corresponding to n fixed spatial frequencies with uniform spacing $\Delta\theta_o^{\text{az}} = \frac{1}{n_{\text{az}}}$ and $\Delta\theta_o^{\text{el}} = \frac{1}{n_{\text{el}}}$ in azimuth and elevation [5], [6], [11]:

$$\mathbf{U}_o = \frac{1}{\sqrt{n}} [\mathbf{a}_n(i\Delta\theta_o^{\text{az}}, \ell\Delta\theta_o^{\text{el}})]_{i \in \mathcal{I}(n_{\text{az}}), \ell \in \mathcal{I}(n_{\text{el}})} \quad (9)$$

that represent n orthogonal beams covering the spatial horizon ($-\frac{\pi}{2} \leq \phi^{az} \leq \frac{\pi}{2}, -\frac{\pi}{2} \leq \phi^{el} \leq \frac{\pi}{2}$), forming a basis for the n -dimensional spatial signal space. In fact, \mathbf{U}_o is a unitary matrix (representing the Kronecker product of DFT matrices in azimuth and elevation): $\mathbf{U}_o^H \mathbf{U}_o = \mathbf{U}_o \mathbf{U}_o^H = \mathbf{I}$.

The beamspace system representation is obtained by choosing $\mathbf{G} = \mathbf{U}_o \mathbf{G}_b$ in (2)

$$\mathbf{r} = \mathbf{H}_b^H \mathbf{G}_b \mathbf{s}_b + \mathbf{w}, \quad \mathbf{H}_b = \mathbf{U}_o^H \mathbf{H} = [\mathbf{h}_{b,1}, \dots, \mathbf{h}_{b,K}] \quad (10)$$

where $\mathbf{s}_b = \mathbf{s}$ represents the beamspace symbol vector and \mathbf{G}_b is the beamspace precoder. $\mathbf{x}_b = \mathbf{G}_b \mathbf{s}_b$ represents the precoded beamspace transmit signal vector. Since \mathbf{U}_o is a unitary matrix, the beamspace channel matrix \mathbf{H}_b is a completely equivalent representation of \mathbf{H} .

C. AP Configurations and Beam Footprints

The most important property of \mathbf{H}_b is its structure reflecting the locations of the different MSs. As illustrated in Fig. 2(b) and (c), where the grid lines represent the beamspace sample points, the dominant entries of \mathbf{H}_b reflect the LoS directions of the MSs ($\theta_k^{az}, \theta_k^{el}$). For an UPA of dimension $n = n_{az} \times n_{el}$ the spatial frequencies where the $(i, \ell)^{\text{th}}$ orthogonal beam is dominant correspond to the set $\mathcal{S}_{i,\ell} = \mathcal{S}_i^{az} \times \mathcal{S}_\ell^{el}$ where

$$\mathcal{S}_i^{az} = \{\theta^{az} \in [i\Delta\theta_o^{az} - \Delta\theta_o^{az}/2, i\Delta\theta_o^{az} + \Delta\theta_o^{az}/2]\} \quad (11)$$

and \mathcal{S}_ℓ^{el} is defined similarly. The beam footprints are the mapping of the $\mathcal{S}_{i,\ell}$ to points on the $x-y$ plane in Fig. 2(a). For a given AP configuration $(n_{az}, n_{el}, h, \psi)$ this mapping is given by the function $(x, y) = g(\theta^{az}, \theta^{el})$ defined by

$$\begin{aligned} x &= h \frac{\sqrt{1-4\theta^{el2}} \cos \psi + 2\theta^{el} \sin \psi}{\sqrt{1-4\theta^{el2}} \sin \psi - 2\theta^{el} \cos \psi} \\ y &= h \frac{2\theta^{az}}{\sqrt{1-4\theta^{az2}} \sin \psi - 2\theta^{el} \frac{\sqrt{1-4\theta^{az2}}}{\sqrt{1-4\theta^{el2}}} \cos \psi} \end{aligned} \quad (12)$$

The footprint for the $(i, \ell)^{\text{th}}$ orthogonal beam is

$$\mathcal{F}_{i,\ell} = \{(x, y) = g(\theta^{az}, \theta^{el}) : (\theta^{az}, \theta^{el}) \in \mathcal{S}_{i,\ell}\}. \quad (13)$$

For a fixed AP configuration $(n_{az}, n_{el}, h, \psi)$, we define the set beam indices \mathcal{M}_{cell} as

$$\mathcal{M}_{cell} = \{(i, \ell) : \mathcal{F}_{i,\ell} \cap \mathcal{C} \neq \emptyset\}. \quad (14)$$

where \mathcal{C} is the set of (x, y) points in the cell sector. That is, \mathcal{M}_{cell} represents the $p = |\mathcal{M}_{cell}|$ beams (out of n orthogonal beams supported by the UPA) that fall within the cell sector and form the communication modes of the MU-MIMO link. Fig. 3 shows this for a cell with $R_{min} = 10$ m, $R_{max} = 100$ m, and $\eta_{max} = 60^\circ$ for six AP configurations $(n_{az}, n_{el}, h, \psi)$.

D. Oversampling the Cell

When communicating with K MSs, choosing an AP configuration with $p = K$ beams in the cell sector is the minimal requirement for spatial multiplexing (Fig. 3(a)-(c) for $K = 100$ MSs). However, increasing the UPA dimension to oversample the cell sector so that $p = |\mathcal{M}_{cell}| > K$

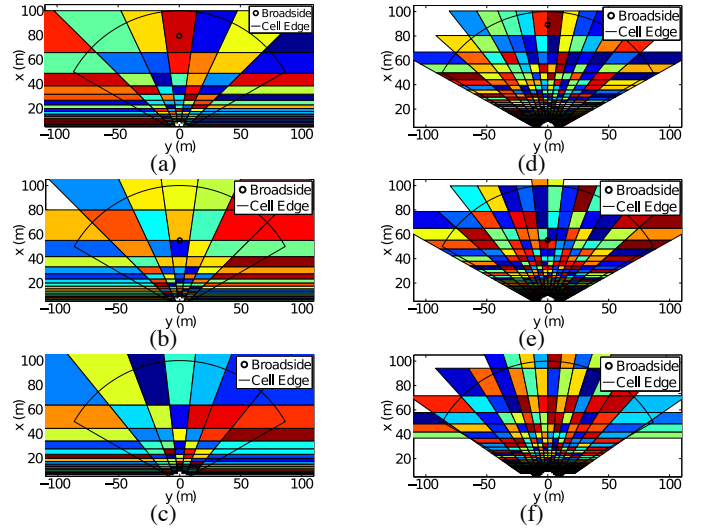


Fig. 3: Beam footprints for a cell with $R_{min}=10$ m, $R_{max}=100$ m, and $\eta_{max} = 60^\circ$ and different AP configurations: (a) $(n_{az}, n_{el}, h, \psi) = (7, 39, 10\text{m}, 7.2^\circ)$, (b) $(7, 36, 10\text{m}, 10.3^\circ)$, (c) $(7, 34, 10\text{m}, 37^\circ)$, (d) $(16, 81, 10\text{m}, 6.4^\circ)$, (e) $(16, 76, 10\text{m}, 10.3^\circ)$, and (f) $(16, 70, 10\text{m}, 37^\circ)$. $p \approx 100 = K$ for (a)-(c) and $p \approx 400 = 4K$ for (d)-(f).

($p = 4K$ in Fig. 3(d)-(e) for $K = 100$ MSs) can improve performance by increasing array gain and limiting interference through narrower beams. Now many of the beam footprints will not cover a MS and the beamspace channel will be sparse (compare Fig. 2(c) with $p = 16K$ to Fig. 2(b) with $p = K$), which can be exploited for complexity reduction. For the oversampled case ($p > K$) we define the following sets of beam indices – *sparsity masks* – that represent the $K \leq \tilde{p} = |\mathcal{M}| < p = |\mathcal{M}_{cell}|$ dominant beams that are selected for transmission at the AP

$$\begin{aligned} \mathcal{M}_k &= \left\{ (i, \ell) \in \mathcal{M}_{cell} : |h_{b,k}(i, \ell)|^2 \geq \gamma_k \max_{(i,\ell)} |h_{b,k}(i, \ell)|^2 \right\} \\ \mathcal{M} &= \bigcup_{k=1, \dots, K} \mathcal{M}_k \end{aligned} \quad (15)$$

where \mathcal{M}_k is the sparsity mask for the k^{th} MS, determined by the threshold $\gamma_k \in (0, 1)$. In this paper we use the m -beam mask [9], i.e. each γ_k is selected so that \mathcal{M}_k selects the m -dominant beams for the k^{th} MS, resulting in $\tilde{p} \leq mK$. Specifically, we use a 4-beam mask since we expect each LoS MSs direction to have at most 4 dominant entries in $\tilde{\mathbf{H}}$ (c.f. the 2-beam mask used in [9] for ULAs)

For a fixed AP configuration $(n_{az}, n_{el}, h, \psi)$, selecting the beams in \mathcal{M}_{cell} (or \mathcal{M}) for data transmission is equivalent to selecting a subset of p (or \tilde{p}) rows of \mathbf{H}_b resulting in the following low dimensional system equation

$$\mathbf{r} = \tilde{\mathbf{H}}_b^H \tilde{\mathbf{G}}_b \mathbf{s}_b + \mathbf{w}, \quad \tilde{\mathbf{H}}_b = [\mathbf{H}_b(\ell, :)]_{\ell \in \mathcal{M}_{cell}(\mathcal{M})} \quad (16)$$

where $\tilde{\mathbf{H}}_b$ is the $p \times K$ (or $\tilde{p} \times K$) beamspace channel matrix corresponding to the selected beams and $\tilde{\mathbf{G}}_b$ is the corresponding $p \times K$ (or $\tilde{p} \times K$) precoding matrix.

E. Minimum Dimension Conventional MIMO Array

The above analysis suggests that the dimension of the UPA in a conventional MIMO system can be reduced -

thereby reducing the complexity. Let ϕ_{max}^{az} denote the maximum (positive or negative) one-sided azimuth angular spread. The maximum normalized inter-element spacing \tilde{d} satisfies $\tilde{d} \sin \phi_{max}^{az} = 1/2$, ensuring that points in the cell sector will have a 1-1 mapping to $[-0.5, 0.5]$ in spatial frequency, so all the beams excited by the array will be in the sector¹ [5]. Since the array size $L^{az} = (n_{az} - 1)/2 = (\tilde{n}_{az} - 1)\tilde{d}$ is constant, the number of \tilde{d} spaced elements in the azimuth is

$$\tilde{n}_{az} = (n_{az} - 1) \sin \phi_{max}^{az} + 1. \quad (17)$$

Similarly for a maximum elevation angular spread of ϕ_{max}^{el}

$$\tilde{n}_{el} = (n_{el} - 1) \sin \phi_{max}^{el} + 1. \quad (18)$$

Thus the total dimension of the minimum dimension conventional MIMO array is $\tilde{n} = \tilde{n}_{az} \times \tilde{n}_{el}$.

F. Software and Hardware Complexity

As discussed in [9], the MIMO processing complexity of linear precoding for a $q \times K$ channel is $\mathcal{O}(q)$. For a fixed AP configuration, the low-complexity B-MIMO precoders will result in a complexity reduction from $\mathcal{O}(n)$ for conventional MIMO transceivers using a critically spaced UPA to $\mathcal{O}(p)$ (beam selection via \mathcal{M}_{cell}) or $\mathcal{O}(\tilde{p})$ (beam selection via \mathcal{M}). With an analog beamforming front-end, as in CAP-MIMO [5], [6], this also dramatically reduces the transceiver hardware complexity (the number of RF chains, including mixers, D/A or A/D converters, and amplifiers) from $\mathcal{O}(n)$ to $\mathcal{O}(p)$ or $\mathcal{O}(\tilde{p})$. An important distinction between \mathcal{M}_{cell} and \mathcal{M} is that while \mathcal{M}_{cell} is only determined by the cell geometry, \mathcal{M} depends on the channel realization (MS locations). Thus while beam selection via \mathcal{M} results in complexity reduction that tracks the number of MSs rather than the UPA dimension, it requires the addition of a beam-switching mechanism.

III. PERFORMANCE AND NUMERICAL RESULTS

In this section we assess the performance of small cell systems using B-MIMO transceivers. Based on the results of [9], we use Wiener filter (WF) precoding. The low-complexity B-MIMO WF precoder is given by [15]–[17]

$$\tilde{\mathbf{G}}_b = \alpha \mathbf{F} = \alpha [\mathbf{f}_1, \mathbf{f}_2, \dots, \mathbf{f}_K], \quad \alpha = \sqrt{\frac{\rho}{\text{tr}(\mathbf{F} \mathbf{\Lambda}_s \mathbf{F}^H)}} \quad (19)$$

$$\mathbf{F} = (\tilde{\mathbf{H}}_b \tilde{\mathbf{H}}_b^H + \zeta \mathbf{I})^{-1} \tilde{\mathbf{H}}_b, \quad \zeta = \sigma^2 K / \rho \quad (20)$$

We assess the conditional sum capacity for a given channel realization (random MS locations $\{R_k, \eta_k\}$) as

$$C(\rho | \tilde{\mathbf{H}}_b) = \sum_{k=1}^K \log_2(1 + \text{SINR}_k(\rho | \mathbf{H})) \text{ bits/s/Hz} \quad (21)$$

where the interference is treated as noise and the signal-to-interference-and-noise (SINR) ratio for the k^{th} MS is

$$\text{SINR}_k(\rho | \tilde{\mathbf{H}}_b) = \frac{\rho \frac{|\alpha|^2}{K} |\mathbf{h}_k^H \mathbf{f}_k|^2}{\rho \frac{|\alpha|^2}{K} \sum_{m \neq k} |\mathbf{h}_k^H \mathbf{f}_m|^2 + \sigma^2}. \quad (22)$$

¹While some of the beams excited by the array will have grating lobes outside of the sector, the greater than critical spacing allows the array element pattern to be selected to minimize energy radiated outside the cell sector

The ergodic sum capacity is determined by averaging over channel realizations as $C(\rho) = E[C(\rho | \tilde{\mathbf{H}}_b)]$.

A. Simulation Environment

We fix the number of MSs at $K = 100$ and distribute them in a 120° sector ($\eta_{max} = 60^\circ$) of a cell defined by $R_{min} = 10$ m and $R_{max} = 100$ m. We fix the AP height at $h = 10$ m and consider three cases of ψ that result in 1) the array broadside pointing near the cell edge (Fig. 3(a) and (d)), 2) the array broadside pointing at the center of the cell (Fig. 3(b) and (e)), 3) equal positive and negative elevation one-sided angular spreads (Fig. 3(c) and (f)). For each case of ψ , we first select the UPA dimensions (n_{az}, n_{el}) according to the minimal requirement $p \approx 100 = K$ (Table 1. AP config. 1–3, Fig. 2(a), and Fig. 3(a)-(c)). Then we increase the UPA dimensions by a factor of 2 in azimuth and elevation to obtain $p \approx 400 = 4K$, which is the case where the complexity of using the 4-beam mask and using all the beams in \mathcal{M}_{cell} are approximately equal (Table 1. AP config. 4–6 and Fig. 3(d)-(f)). Finally, the UPA dimensions are increased by an additional factor of 2 to obtain $p \approx 1600 = 16K$ (Table 1. AP config. 7–9 and Fig. 2(c)). Table 1 lists the AP configurations, as well as the corresponding UPA dimensions for the minimum dimension conventional array and the array size at 80 GHz.

The free space path loss values for points in the cell sector range from -93.5 dB to -110.5 dB at 80 GHz. Thus, considering transmit SNR (ρ/σ^2) values of 52 dB to 112 dB (in Fig. 4 and 5) roughly corresponds to SNRs of -40 dB to 20 dB in Fig. 1(c). With 8 GHz bandwidth the thermal noise power is $\sigma^2 = -72$ dBm, so these transmit SNRs correspond to transmit powers of $-20 - 40$ dBm (0.01 mW – 10 W).

AP config.	ψ ($^\circ$)	n_{az}	n_{el}	n	p	\tilde{n}_{az}	\tilde{n}_{el}	\tilde{n}	Array Size at 80 GHz
1	7.2	7	39	273	105	7	32	224	0.45"×2.81"
2	10.3	7	36	245	103	7	29	203	0.45"×2.58"
3	37	7	34	238	100	7	19	133	0.45"×2.44"
4	6.4	16	81	1296	408	15	66	990	1.11"×5.91"
5	10.3	16	76	1216	402	15	61	915	1.11"×5.54"
6	37	16	70	1120	404	16	39	624	1.11"×5.09"
7	6	32	163	5216	1610	29	138	4002	2.29"×11.96"
8	11.1	32	157	5024	1600	29	122	3538	2.29"×11.52"
9	37	32	151	4832	1614	31	81	2511	2.29"×11"

TABLE I: AP configurations

B. Numerical Results

Fig. 4 shows the ergodic sum capacity, generated by averaging over 10000 channel realizations, for the AP configurations in Table 1 when all p beams in \mathcal{M}_{cell} are used. The MSs are uniformly randomly placed within the cell sector, the path amplitudes are calculated via (8) numerically for a frequency of 80 GHz with phases ϕ_k uniformly distributed in $[0, 2\pi]$.

The figure shows the capacity increases as the UPA dimension increases as expected. From the $4 \times$ increase in array size between AP configs 1-3 and 4-6 and between AP configs 4-6 and 7-9, we expect an ≈ 6 dB gap between the curves if the improvement is only due to increased array gain. Since the gaps are significantly larger it is clear that much of the capacity gain comes from the reduced interference caused by the narrower beams. Case 1) of ψ gives the best performance,

although the performance of case 2) is not significantly worse. This indicates that while properly selecting ψ is important, tilt angle errors of a few degrees are acceptable.

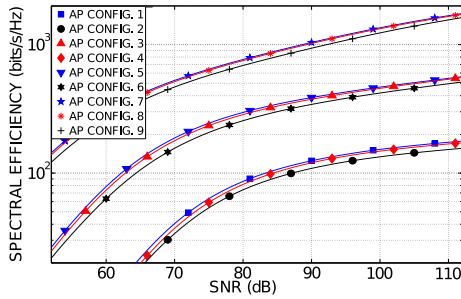


Fig. 4: Sum capacity of the various AP configurations.

Configuration 7 provides the best performance, however transmitting on the $p = 1610$ in beams in \mathcal{M}_{cell} results in a fairly complex transceiver. Thus, we use a 4-beam sparsity mask for complexity reduction. Fig. 5 compares the capacity of configuration 7 with and without the 4-beam mask, showing that their performances are closely matched due to beamspace sparsity. This shows that when using the low-complexity B-MIMO transceivers with the 4-beam mask and increasing the AP dimension to limit interference and increase array gain, the complexity remains at $\mathcal{O}(400) = \mathcal{O}(4K)$ tracking the number of MSs. In contrast, the complexity of conventional MIMO transceivers, even with the minimum dimension array, continues to track the array dimension n .

At an SNR of 92 dB the capacity of the transceiver using the 4-beam mask is 1067 bits/s/Hz. For a system using 8 GHz of bandwidth, this corresponds to an aggregate rate of 8536 Gbps or an average per user rate of about 85 Gbps with a transmit power of 20 dBm. Currently, LTE Advanced using 8×8 MIMO spatial multiplexing can provide a peak downlink rate of 3.3 Gbps over a 100 MHz bandwidth under ideal conditions [18]. Thus the combination of the $80 \times$ increase in bandwidth, the increased array gain, and the dense spatial multiplexing of $K = 100$ MSs results in a more than $1000 \times$ increase in the downlink rate. However, since the 4-beam mask is used for complexity reduction, when using a system with an analog beamforming front-end, e.g. CAP-MIMO [5], [6], there is only a $50 \times$ increase in transceiver hardware complexity (8 to 400).

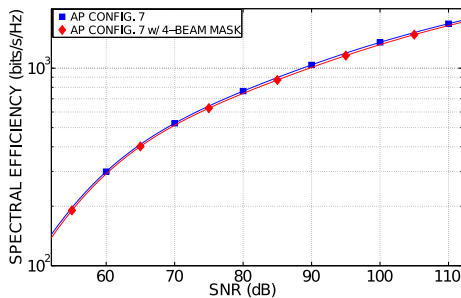


Fig. 5: Sum capacity for AP config. 7 with and without the 4-beam mask.

IV. CONCLUSIONS

We have presented a study on the application of low complexity B-MIMO transceivers to small cell MU-MIMO systems operating at mm-wave. Using a realistic LoS channel

model, we first apply the B-MIMO theory to analyze the small cell in terms of the beam footprints. We then analyze the performance of the transceivers communicating with $K = 100$ MSs in a 120° sector of a 100 m small cell for several AP configurations. We demonstrate that increasing the UPA dimension results in dramatic performance gains due to the narrower beams. Furthermore, using the 4-beam mask allows the UPA dimension to be increased while keeping the transceiver complexity at $\mathcal{O}(4K)$, independent of the array dimension n . Thus, the low-complexity B-MIMO transceivers provide the near-optimal route for exploiting the narrow, high gain beams at mm-wave to provide 1000s of Gbps rates over 100s of MSs with minimum system complexity. However realizing these gains in practical transceivers will require further research, including the development of efficient beamspace channel estimation algorithms and analog beam-switching schemes.

REFERENCES

- [1] N. Bhushan, Junyi Li, D. Malladi, R. Gilmore, D. Brenner, A. Damnjanovic, R. Sukhavasi, C. Patel, and S. Geirhofer, "Network densification: the dominant theme for wireless evolution into 5G," *IEEE Comm. Mag.*, vol. 52, no. 2, pp. 82–89, February 2014.
- [2] B. Bangerter, S. Talwar, R. Arefi, and K. Stewart, "Networks and devices for the 5G era," *IEEE Comm. Mag.*, vol. 52, no. 2, pp. 90–96, Feb. 2014.
- [3] V. Chandrasekhar, J.G. Andrews, and A. Gatherer, "Femtocell networks: a survey," *IEEE Comm. Mag.*, vol. 46, no. 9, pp. 59–67, Sept. 2008.
- [4] J.G. Andrews (moderator), "The Rapid Evolution of Cellular Networks: Femto, Pico and all that," in *Proc. 2011 Texas Wireless Summit (panel discussion)*, Oct. 2011.
- [5] A. M. Sayeed and N. Behdad, "Continuous Aperture Phased MIMO: Basic Theory and Applications," in *Proc. Allerton Conf.*, Sept. 29-Oct. 1 2010, pp. 1196–1203.
- [6] A. M. Sayeed and N. Behdad, "Continuous Aperture Phased MIMO: A new architecture for optimum line-of-sight links," in *Antennas and Propagation, 2011 IEEE Int. Symp.*, July 2011, pp. 293–296.
- [7] Z. Pi and F. Khan, "An Introduction to Millimeter-Wave Mobile Broadband Systems," *IEEE Comm. Mag.*, vol. 49, no. 6, pp. 101–107, June 2011.
- [8] T. L. Marzetta, "Noncooperative Cellular Wireless with Unlimited Numbers of Base Station Antennas," *IEEE Trans. Wireless Comm.*, vol. 9, no. 11, pp. 3590–3600, Nov. 2010.
- [9] A. Sayeed and J. Brady, "Beamspace MIMO for High-Dimensional Multiuser Communication at Millimeter-Wave Frequencies," in *Globecom 2013*, Dec 2013, pp. 3785–3789.
- [10] D. Gesbert, M. Kountouris, R. Heath, C.B. Chae, and T. Salzer, "Shifting the MIMO paradigm," *IEEE Signal Processing Mag.*, vol. 24, no. 5, pp. 36–46, Sep. 2007.
- [11] A. M. Sayeed, "Deconstructing Multiantenna Fading Channels," *IEEE Trans. Signal Process.*, vol. 50, no. 10, pp. 2563–2579, Oct. 2002.
- [12] T. S. Rappaport, E. Ben-Dor, J. N. Murdock, and Y. Qiao, "38 GHz and 60 GHz Angle-dependent Propagation for Cellular & Peer-to-Peer Wireless Communications," in *2012 IEEE Int. Conf. on Communications (ICC)*, June 2012, pp. 4568–4573.
- [13] H.T. Friis, "A Note on a Simple Transmission Formula," *Proceedings of the IRE*, vol. 34, no. 5, pp. 254–256, May 1946.
- [14] Constantine A. Balanis, *Antenna Theory: Analysis and Design*, Wiley-Interscience, 2005.
- [15] M. Joham, W. Utschick, and J.A. Nossek, "Linear transmit processing in MIMO communications systems," *IEEE Trans. Signal Process.*, vol. 53, no. 8, pp. 2700–2712, Aug. 2005.
- [16] A. Sayeed and T. Sivanadayan, "Wireless Communication and Sensing in Multipath Environments with Multi-antenna Wireless Transceivers," in *Handbook on Array Processing and Sensor Networks 1st ed.*, K. J. R. Liu and S. Haykin, Eds., pp. 115–170. IEEE-Wiley, Hoboken, NJ, 2010.
- [17] T. Sivanadayan and A. Sayeed, "Space-time reversal techniques for wideband MIMO communication," in *Signals, Systems and Computers, 2008 42nd Asilomar Conf. on*, Oct 2008, pp. 2038–2042.
- [18] M. Rummey ed., *LTE and the Evolution to 4G Wireless: Design and Measurement Challenges, 2nd Edition*, Wiley, 2013.